PERGAMON

International Journal of Heat and Mass Transfer 43 (2000) 901–919

International Journal of HEAT and MASS TRANSFER

www.elsevier.com/locate/ijhmt

Flow transition in a multilouvered fin array

D.K. Tafti*, G. Wang [1], W. Lin [2]

National Center for Supercomputing Applications, University of Illinois at Urbana-Champaign, Urbana, IL 61801, USA

Received 10 September 1998; received in revised form 24 May 1999

Abstract

The paper describes the detailed transition mechanism from steady to unsteady flow in a multilouvered fin geometry. The initial instability appears in the wake of the exit louver at a Reynolds number of 400 with a characteristic non-dimensional frequency (based on inflow velocity and louver pitch) of 0.84. Between a Reynolds number of 700 and 800, power spectra in the interior of the array indicate an increase in energy in the vicinity of the first harmonic of the initial exit wake instability. By a Reynolds number of 900, free shear layer or Kelvin–Helmholtz type instabilities develop on the leading edge shear layers of louvers near the exit. These instabilities have a characteristic non-dimensional frequency of 1.7. As the Reynolds number increases further, instabilities move upstream into the array. By a Reynolds number of 1300, most of the louvers exhibit unsteadiness, except for the entrance louver and the first two louvers following it. By this Reynolds number, the flow in the downstream half of the array exhibits a chaotic behavior.

1. Introduction

During the past two decades, much effort had been made to understand the flow phenomena and performance characteristics in louvered fin arrays. Two kinds of flow regimes have been observed in flow visualizations [1,2]. At low Reynolds numbers the flow is nearly parallel to the axial direction (duct flow) whereas at high Reynolds number the flow is in the direction of the louvers. These two regimes have been found to have a profound impact on the heat transfer characteristics. The duct flow regime has been found to be responsible for the flattening characteristics of the Nusselt number at low Reynolds numbers [2]. Another mechanism, which has a profound effect on heat transfer is the onset of unsteadiness. Transition to unsteadiness results in the presence of large scale vortical structures which considerably enhance heat transfer [3,4]. A better understanding of the onset and propagation of instabilities in a multilouvered fin array has potential applications in the design of more efficient and application specific multilouvers. This is particularly relevant in light that for most applications the transitional regime is present for a large part of the operating range of the heat exchanger.

In spite of the importance of understanding the transitional nature of the flow in louvered fin arrays, there have been very few studies devoted to this aspect. There are scattered references in the literature to the onset of unsteadiness in louvered fin arrays, most of which are based on experimental flow visualization [5,6]. Recently, Springer and Thole [7] have performed hot wire measurements in a multilouvered array and identified the onset of unsteadiness and the characteristic frequency. On the other hand, most compu-

* Corresponding author.

[1] Present address: Development Department, ANSYS Inc, Southpointe, 275 Technology Drive, Canonsburg, PA 15317, USA

[2] Present address: Emerson Ventilation Products, 10048 Industrial Boulevard, Lenexa, KS 66215, USA

0017-9310/00/$ - see front matter
PII: S0017-9310(99)00190-8

Nomenclature

$\vec{a}^1, \vec{a}^2$	contravariant basis vectors
b	fin thickness
f	characteristic frequency
$\sqrt{g}$	Jacobian of transformation
g^{ij}	contravariant metric tensor
p	pressure
t	time
u, v	Cartesian velocity in x- and y-directions
x, y	physical space
F	fin pitch
L	louver pitch
L_x	basic computational unit length in x-direction
L_y	basic computational unit length in y-direction
Pr	Prandtl number
Re	Reynolds number
S_{u_i}	source term in momentum equations
S_T	source term in energy equation
S_1, S_2	entrance/exit and redirection louver dimensions
T	temperature
U, V	contravariant fluxes in ξ- and η-coordinates

Greek symbols

α	louver angle
ν	kinematic viscosity
ξ,η	transformed coordinates

Superscripts

*	dimensional quantities

Subscripts

in	based on inlet

tational studies of louvered fins have been confined to the laminar flow assumption [8–12] and the use of the RANS approach with turbulence models to model unsteady motions [13]. While experimental studies have some inherent difficulties is studying spatial transition and propagation, numerical studies, which are well suited for this exercise, are mainly limited by computational resources. To capture the transition with accuracy mandates that both temporal and spatial scales be resolved with accuracy. Fortunately, in the early stages of transition the flow can be assumed to be intrinsically two-dimensional without compromising the important physics.[3] For developing flow in a multilouvered array, even two-dimensional calculations over a range of geometries and flow parameters can be quite challenging and requires the use of state-of-the-art computational hardware and associated software infrastructure.

Three possible mechanisms could potentially contribute to the transition to unsteadiness in the multilouvered flow geometry. The first instability mechanism is the wake instability as observed in vortex shedding from square and circular cylinders, and from rectangular cylinders similar to louvers. This instability occurs in the presence of two shear layers, which are primarily responsible for vortex shedding [14]. The unsteadiness is characterized by the classical Von Karman vortex street [15]. The second potential instability mechanism is the Kelvin–Helmhotz instability or the free-shear-layer instability as observed in the separated and reattaching flow on a blunt flat plate [16–18]. In the current context, these instabilities could develop at the leading edges of individual louvers. For Reynolds numbers (based on approach velocity and plate thickness) greater than 350, the flow field is observed to be unsteady with the formation of spanwise vortices in the separated shear layer. These vortices subsequently coalesce to form larger vortices, which are then shed periodically from the reattachment region. Finally, the third potential instability mechanism is the impinging shear-layer instability (ISLI) as observed in the vortex shedding from elongated rectangular cylinders [19–22]. This instability differs from the Kelvin–Helmholtz and the wake instability in that the separated shear layers from the leading edges impinge on the trailing edges and become unstable. One distinct characteristic for this flow is the stepwise variations of Strouhal number vs the chord (length)-to-thickness ratio when the Reynolds number is above a critical value. Usually, this instability is characterized by plotting the Strouhal number, based on length, as a function of length-to-thickness ratio of the rectangular cylinder for fixed Reynolds number. The observed step changes in Strouhal number which occur at length-to-thickness ratio of 6, 9 and 12 are related to the number of vortices along the length of the rectangle.

In this paper, our objective is to identify the type of instabilities which occur, their characteristics, and spatial propagation within the multilouvered array.

[3] Neglecting three-dimensional geometry effects.

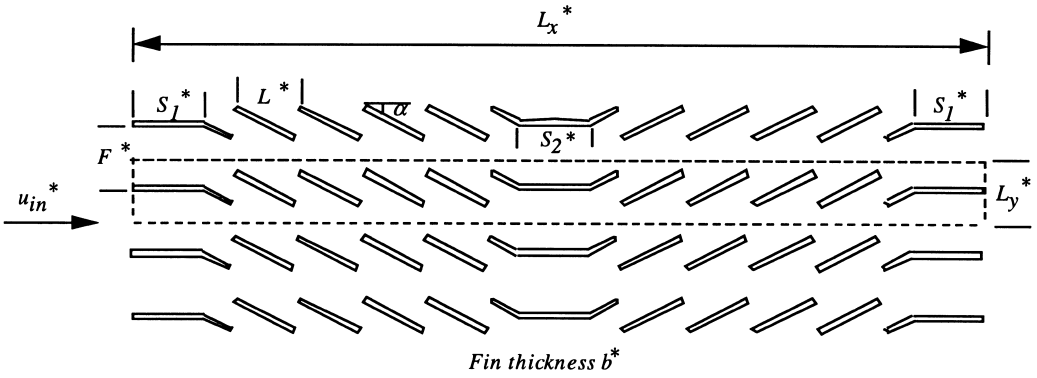

(a)

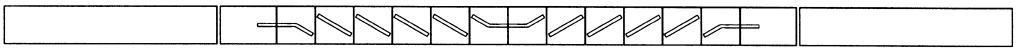

(b)

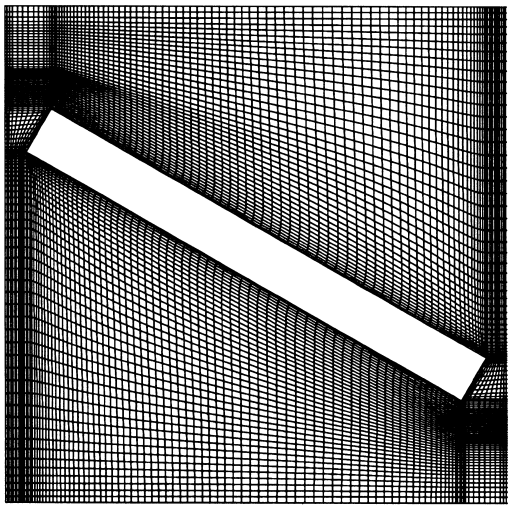

(c)

Fig. 1. (a) Cross-section of multilouvered fin. The dashed lines show the basic computational unit. (b) Multi-block structure with entrance and exit buffer regions. (c) Typical mesh surrounding a louver in a computational block (96 × 96 cells).

2. Governing equations and mathematical formulation

To calculate the flow and thermal fields in the array, we map the Navier–Stokes and energy equations from physical ($\vec{x}$) to logical/computational space ($\vec{\xi}$) by a boundary conforming transformation $\vec{x} = \vec{x}(\vec{\xi})$, where $\vec{x} = (x, y, z)$ and $\vec{\xi} = (\xi, \eta, \zeta)$. Based on the nomenclature of Thompson et al. [23], the transformed *non-dimensional* time-dependent incompressible Navier–Stokes and the energy equations in computational space are written in strong-conservative form as:

Continuity:

$$\frac{\partial}{\partial \xi_j}(\sqrt{g}U^{\ j}) = 0 \tag{1}$$

Momentum:

$$\frac{\partial}{\partial t}(\sqrt{g}u_i) + \frac{\partial}{\partial \xi_j}(\sqrt{g}U^{\ j}u_i) = -\frac{\partial}{\partial \xi_j}(\sqrt{g}(\vec{a}^j)_i p) + \frac{\partial}{\partial \xi_j}\left(\frac{1}{Re}\sqrt{g}g^{jk}\frac{\partial u_i}{\partial \xi_k}\right) + \sqrt{g}S_{u_i}$$

Energy:

$$\frac{\partial}{\partial t}(\sqrt{g}T) + \frac{\partial}{\partial \xi_j}(\sqrt{g}U^{\ j}T) = \frac{\partial}{\partial \xi_j}\left(\frac{1}{PrRe}\sqrt{g}g^{jk}\frac{\partial T}{\partial \xi_k}\right) + \sqrt{g}S_T \tag{3}$$

The governing equations for momentum and energy conservation are discretized with a conservative finite-volume formulation. Both, convection and viscous terms are approximated by second-order central-difference schemes. The computational domain, shown in Fig. 1(a), consists of one entire row of the louvered fin geometry allowing for the inclusion of entrance and exit effects in the flow direction. Periodic boundary conditions are applied in the transverse direction while Dirichlet boundary conditions are specified at the entrance to the array. To facilitate the calculation of the whole array, we use a structured multi-block formulation in the streamwise direction with overlapping boundaries for the application of inter-block boundary conditions. Eqs. (1)–(3) are non-dimensionalized by a characteristic length given by the louver pitch L^*, a characteristic velocity scale given by the inlet velocity to the array (u^*_{in}) and a temperature scale given by ($T^*_{\text{f}} - T^*_{\text{in}}$), where T^*_{f} is the specified fin surface temperature. The non-dimensionalization results in a characteristic Reynolds number $Re = Re_{\text{in}} = u^*_{\text{in}}L^*/\nu$, with Dirichlet boundary conditions $u_{\text{in}} = 1, T_{\text{in}} = 0$ at the entrance to the computational domain. The Prandtl number is fixed at 0.7 for air. At the fin surface, no slip, no penetration boundary conditions for the velocity field, and $T_{\text{f}} = 1$ for the temperature field are applied. Due to the recovering nature of the flow at the array exit, convective boundary conditions of type

$$\frac{\partial \phi}{\partial t} + U^{\ j}\frac{\partial \phi}{\partial \xi_j} = 0 \tag{4}$$

are used at outflow boundary nodes, where ϕ is the convected variable. More details about the time-integration algorithm, treatment of boundary and louver surface conditions, and validation of the computer program can be found in Tafti et al. [24].

3. Computational details

The configuration used in these calculations consists of an entrance and exit louver with four louvers on either side of the center or redirection louver. The non-dimensional geometric parameters are fin pitch $F = 1$, louver thickness $b = 0.1$ and louver angle, $\alpha = 30^\circ$. For the entrance and exit louvers, $S_1 = 1$, and for the center redirection louver, $S_2 = 1$. Fig. 1(b) shows the computational domain which is resolved by 16 blocks, one for each louver, two each for the entrance, exit and redirection louver, and an entrance and exit domain which extend approximately 5.5 non-dimensional units upstream and downstream of the array, respectively. Each block is resolved by 96×96 finite-volume cells. Fig. 1(c), shows a typical mesh distribution in a block surrounding a louver. The pressure equation is converged to 1×10^{-5} based on the average L_1 norm of the residue. Each calculation in the unsteady regime required about 60 h of wall clock time on 16 processors of the SGI/Cray Origin 2000.

In this paper we present results for a Reynolds number range (Re_{in}) of 100 to 1300 in increments of 100. The calculations were started at the lowest Reynolds number, which provided the initial conditions for the subsequent Reynolds number. Each calculation was carefully monitored through pressure drops across blocks, heat transfer, and field variables to determine a stationary state. Stationarity was assumed when time series data of field variables showed a near constant mean value from one run to the next. For the unsteady cases, time averaging was initiated once a stationary state was established. Typically, the unsteady calculations were integrated between 100 and 150 non-dimensional time units. Further, time series data was collected at 64 spatial locations in the computational domain for further analysis. Time series data was collected halfway in the vicinity of the top and bottom surface of each louver, and two locations in the wake of each louver. Based on the time step, the lowest and highest resolved non-dimensional frequencies varied

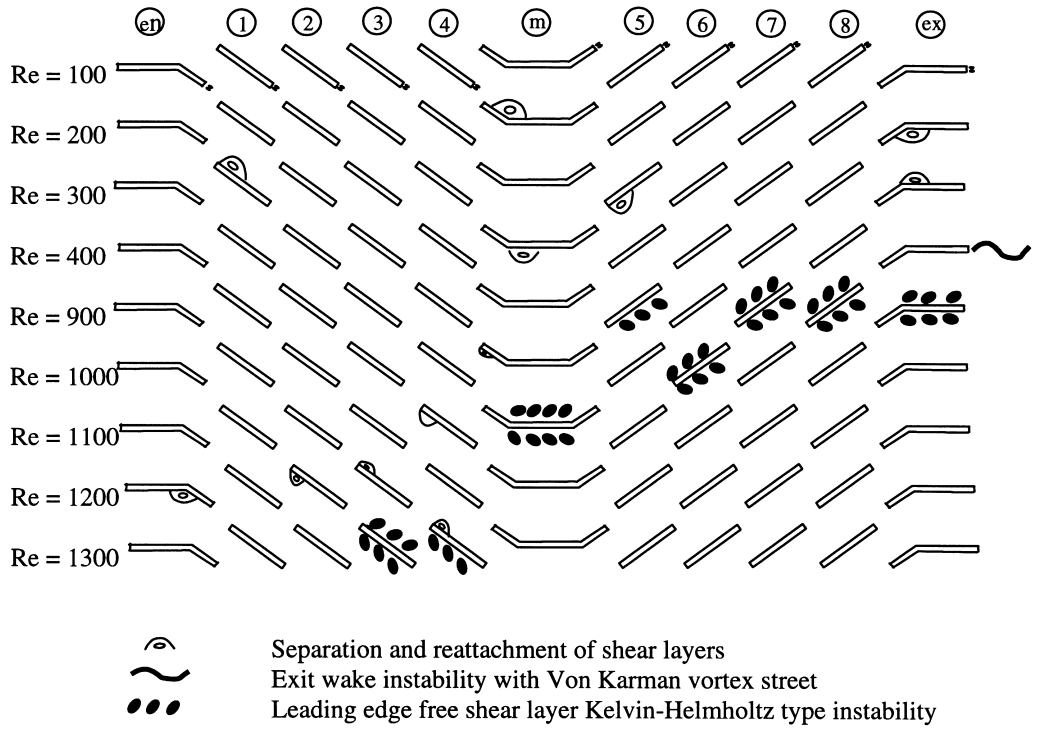

Fig. 2. Development and propagation of instabilities in the multilouvered geometry. Only the initial appearance of instabilities is shown.

between 0.1388–0.042 and 555–167, respectively, in the Reynolds number range $Re_{in} = 400$–1300.

4. Development and propagation of instabilities

The development and propagation of instabilities in the louvered fin array were studied through a combination of flow visualization of instantaneous vorticity and streamline contours over typical shedding cycles and through extensive frequency and time signal analyses. Fig. 2 summarizes the results of this study and shows the sequence of events in the louver array which lead to the transition from a steady laminar flow to laminar unsteady and subsequently to chaotic. The figure only characterizes the initial appearance of features. Although these features persist as the Reynolds number increases, that aspect is not reproduced in the figure for the sake of clarity. It should be stated that Fig. 2 was composed mostly by visual examination of instantaneous flow fields and in some cases by studying animations of vorticity, and hence by definition is qualitative in nature. However, extreme care was taken in producing Fig. 2, with a high degree of confidence in the conclusions made on the spread of instabilities upstream into the array. We attribute a high level of confidence to the *classification* of the initial instabilities that appear in the interior starting at $Re_{in} = 900$. It is only after $Re_{in} > 1000$ and 1100 that the *classification* of instabilities as they move upstream becomes difficult. We say this to caution that once unsteadiness is established for $Re_{in} > 1000$ in the array, the flow field is quite complex and the exact characterization of *type* of instability which occurs on individual louvers is rather difficult. The cause and effect of louver wake and louver leading edge instabilities become difficult to characterize. Fig. 3 characterizes the complexity of the flow by showing plots of instantaneous vorticity at different Reynolds numbers.

At a Reynolds number of 100, small recirculation regions are found to exist in the wake of all the louvers. The wake recirculation bubbles become stronger and larger as the Reynolds number increases. At $Re_{in} = 200$, steady recirculation zones brought about by separation and reattachment are found to exist on the top upstream side of the redirection louver and bottom upstream side of the exit louver. At $Re_{in} = 300$, the shear layers on the leading back sides of louver 1 and louver 5 separate and reattach to form additional recirculation zones. In addition, a recirculation zone also appears on top of the exit louver. As the Reynolds number increases to $Re_{in} = 400$, we find that the wake of the exit louver becomes unstable with clear evidence of the Von Karman vortex street. Fig. 4 shows the in-

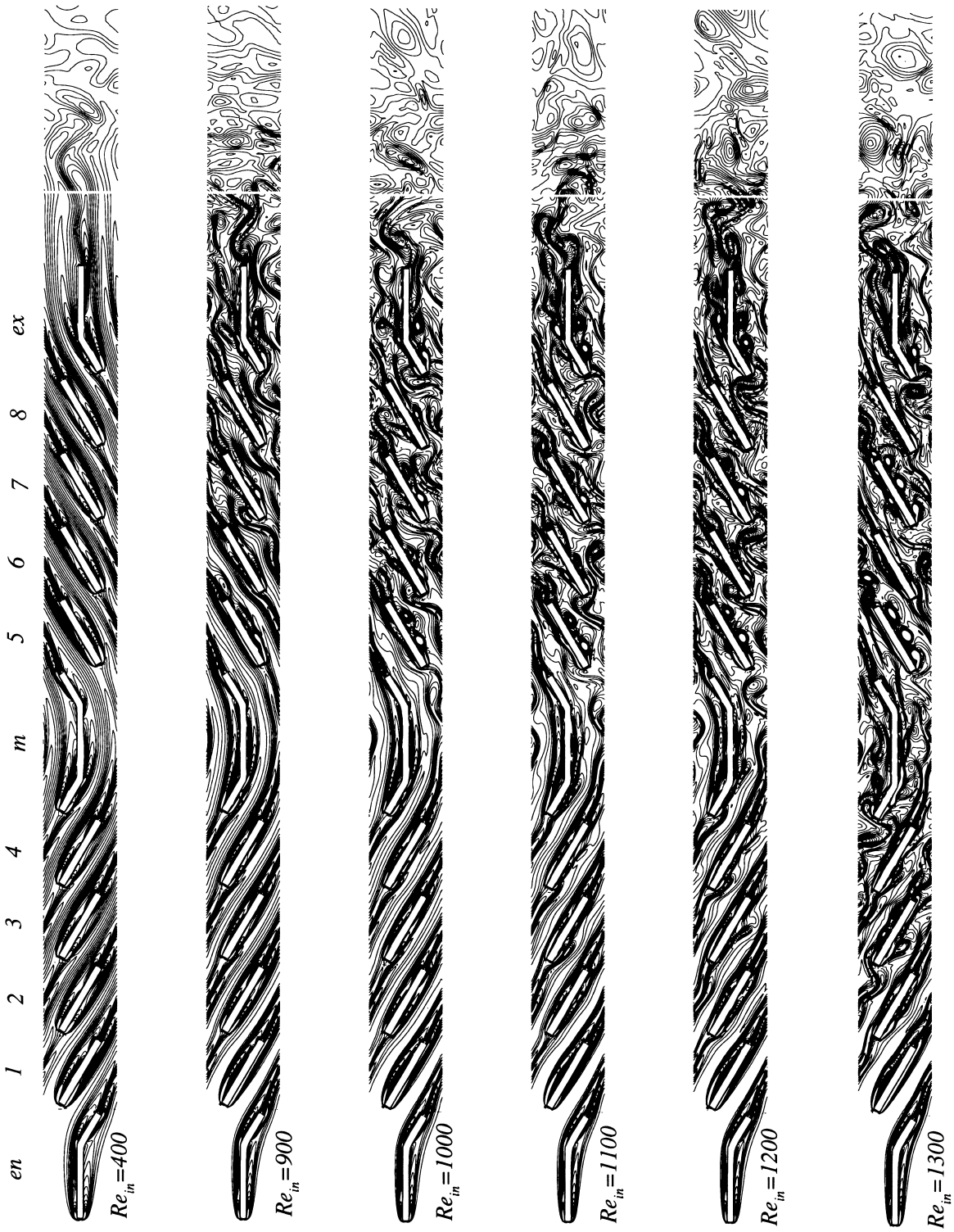

Fig. 3. Instantaneous spanwise vorticity contours.

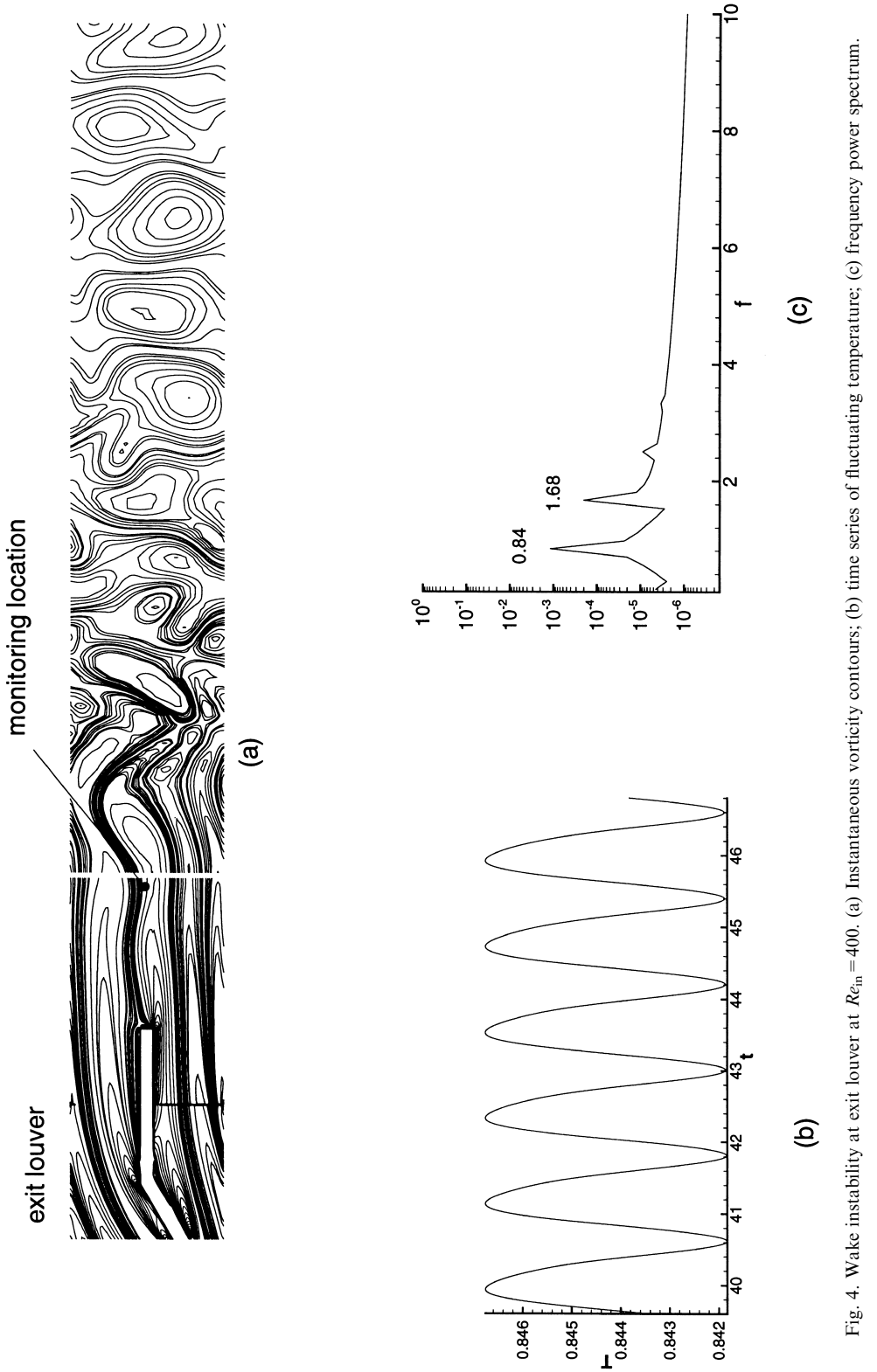

Fig. 4. Wake instability at exit louver at $Re_{in} = 400$. (a) Instantaneous vorticity contours; (b) time series of fluctuating temperature; (c) frequency power spectrum.

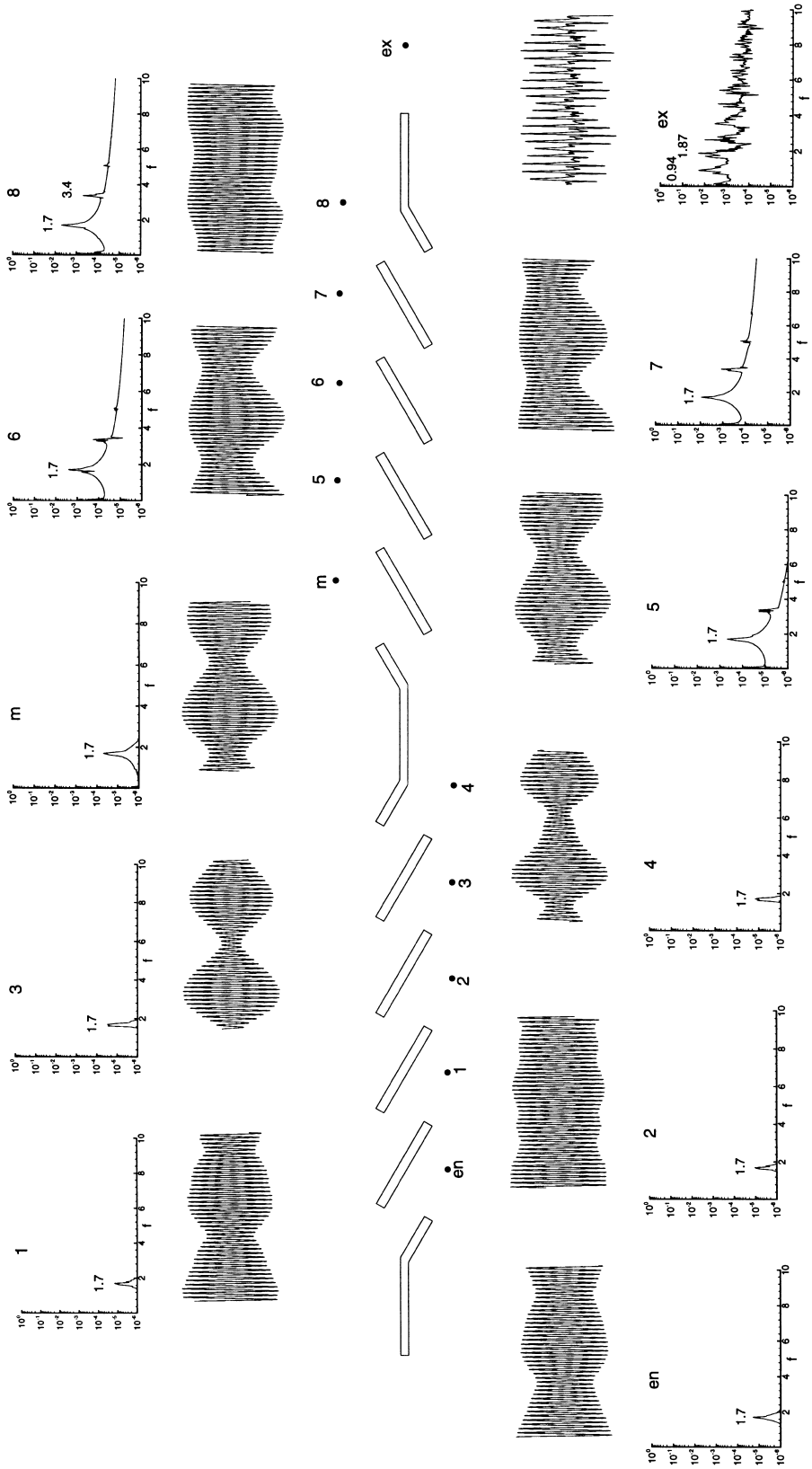

Fig. 5. Spatial distribution of frequency spectra of temperature at $Re_{in}=800$.

Fig. 6. Time series of instantaneous vorticity contours at $Re_{in} = 800$ over one typical cycle based on characteristic frequency of 1.7. Vortices shed from the leading edge shear layers are identified by (+).

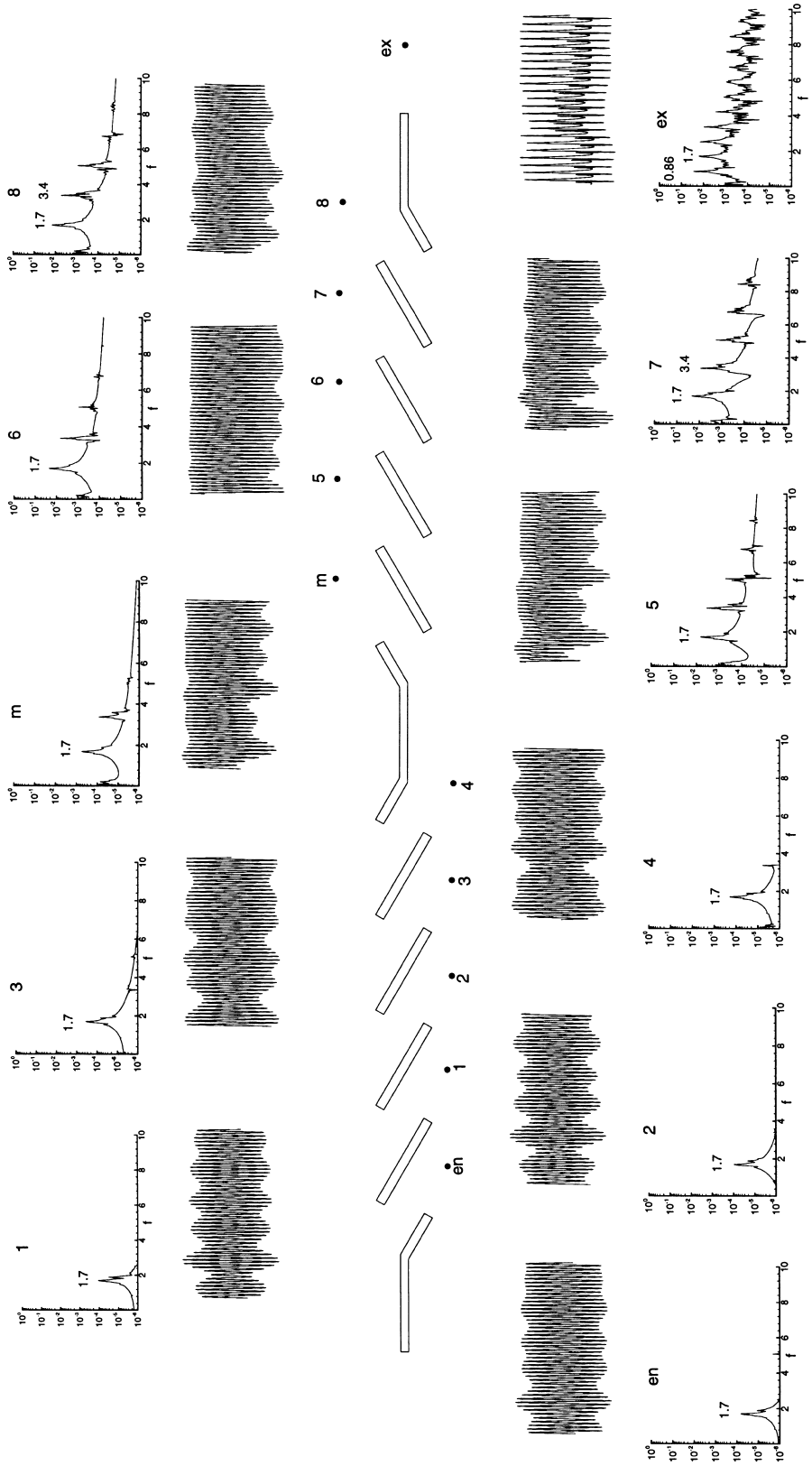

Fig. 7. Spatial distribution of frequency spectra of temperature at $Re_{in}=900$.

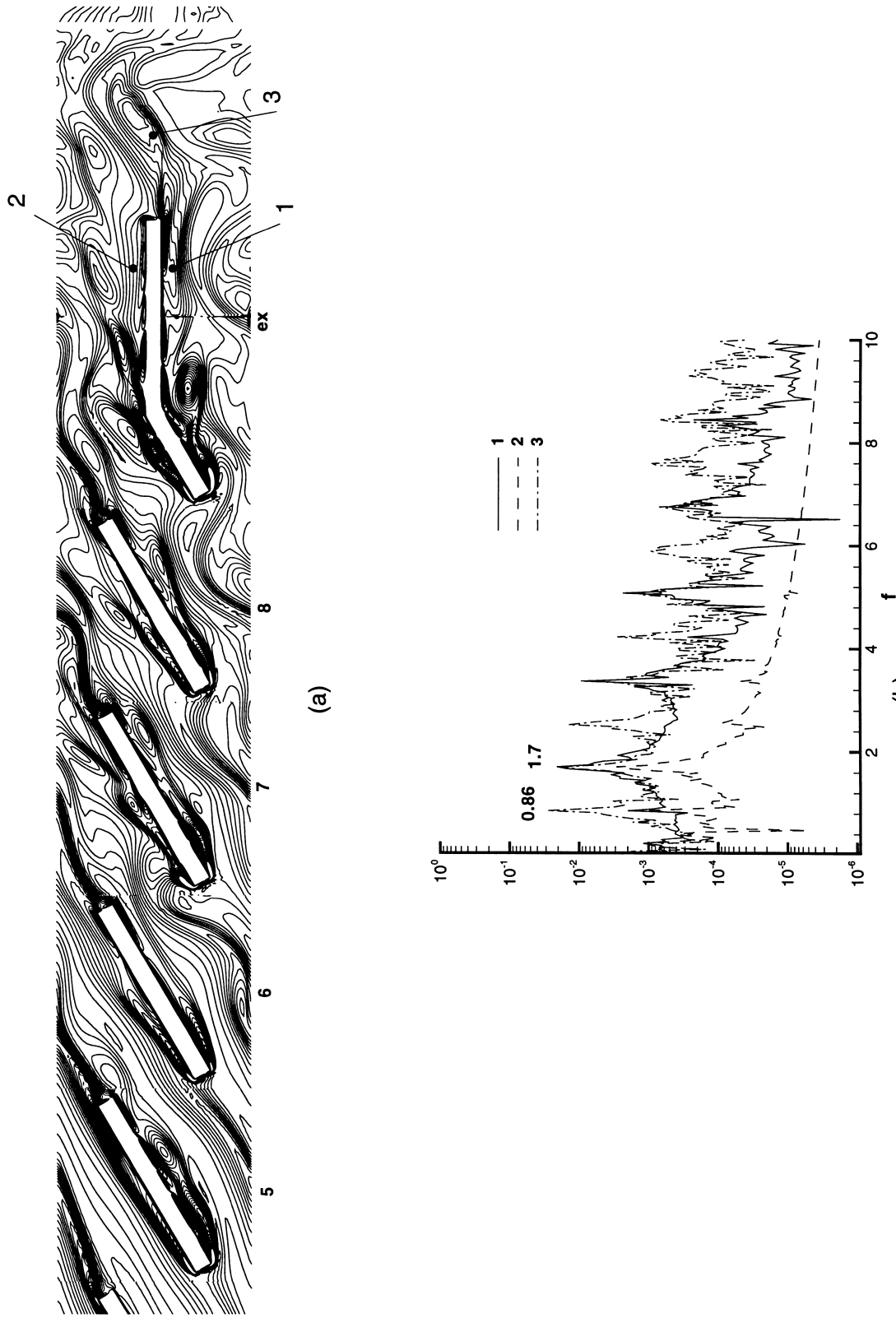

Fig. 8. (a) Instantaneous vorticity contours in downstream half of multilouvered array at $Re_{in}=900$; (b) frequency spectra at three locations in the vicinity of the exit louver.

stantaneous vorticity contours in the wake, together with a representative time signal of temperature and the corresponding frequency power spectrum.[4] We note that although there is a massive separation zone on the top surface of the louver, there is no vortex shedding from the leading edge and it is only in the wake that two shear layers interact and become unstable. However, an interesting aspect is that the instability is caused by the interaction of the leading edge separated shear layer on the top of the exit louver with the trailing edge separated shear at the bottom. In most symmetric bluff body wakes, depending on the after-body from the leading edge, wake interactions are between leading edge or trailing edge shear layers as the case may be. The time signal is periodic with a characteristic non-dimensional frequency, based on louver pitch and the inlet velocity, $f = f^*L^*/u^*_{in} = 0.84$, with a first harmonic at $f_1 = 1.68$. Nakamura et al. [22], performed experiments of uniform flow over blunt rectangular plates of different aspect ratios (thickness to length ratio) at low Reynolds numbers (200–600 based on approach velocity and plate thickness). They observed a wake Strouhal frequency between 0.5 and 2.0 for plates with aspect ratios varying from 2 to 16 at a Reynolds number of 200. We note that the exit louver geometry and the flow conditions are quite different from the experiments. The wake instability generated at the exit louver would effectively be similar to that generated by plates of small aspect ratio. Besides the wake instability, at this Reynolds number, an additional recirculation zone appears on the bottom of the redirection louver as shown in Fig. 2.

As the Reynolds number increases further, visual examination of the flow field does not indicate any other instabilities developing in the array. However, examining frequency spectra in the array indicates that the instability generated in the wake of the exit louver gradually moves into the array. At $Re_{in} = 600$, the characteristic wake frequency increases to $f = 0.92$, with well-defined harmonics established at 1.84, 2.76 and so on. We also find the low amplitude presence (1×10^{-6}) of the fundamental wake frequency and its first harmonic in the wakes of louvers 6 and 7 and 8. At $Re_{in} = 700$, the infiltration of the wake instability (now $f = 0.94$ and $f_1 = 1.87$) into the array increases and moves further upstream. It is also observed that the first harmonic ($f_1 = 1.87$) starts to dominate over the fundamental exit wake frequency in the array interior. However, the typical amplitudes are still of the order of ($1–2 \times 10^{-6}$). We also note that as the Reynolds number increases, the primary wake instability moves closer to the trailing edge of the exit louver.

As the Reynolds number increases to $Re_{in} = 800$, the spectral characteristics inside the array, exhibit a distinct shift from that of the exit wake. The fundamental mode inside the array now exhibits a characteristic frequency of 1.7. Fig. 5 shows the frequency spectra at different locations in the array for $Re_{in} = 800$.[5] Although the exit wake retains the same spectral characteristics as at $Re_{in} = 700$ ($f = 0.94$, $f_1 = 1.87$), the spectra in the interior of the array, as far upstream as the inlet louver, lock on to a frequency of 1.7 and show a marked increase in amplitude. In spite of the observed shift in the spectral characteristics, flow visualization does not indicate any obvious new instability mechanism developed in the array. However, a close look at the exit louver indicates the initial stages of the Kelvin–Helmholtz shear layer instability at the leading edge shear layers of the exit louver. Fig. 6 shows a time sequence of vorticity contours at the exit louver over one typical cycle corresponding to a characteristic frequency of 1.7. Although very weak, there is evidence of vorticity (identified by + in the figure) being shed from the leading edge shear layers. During this time the wake instability goes through little over half a cycle based on $f = 0.94$.

As the Reynolds number increases to 900, the leading edge free shear layer instability establishes itself near the exit of the array. Fig. 7 shows the spatial characteristics of frequency power spectra for $Re_{in} = 900$. The characteristic frequency in the array still maintains its value of 1.7, but flow visualization shows clear evidence of leading edge vortex shedding. The shear layers at the leading edges of louvers 5, 7 and 8 experience a Kelvin–Helmholtz instability, by virtue of which they become unstable and result in the shedding of spanwise vortices. This is seen in Fig. 8(a). Curiously, louver 6 does not exhibit vortex shedding at this Reynolds number. Louver 5 exhibits the instability only on the leading edge of the back surface,[6] while louvers 7 and 8 exhibit vortex shedding on both faces.[7] This is because, the flow coming out of the redirection or middle louver is not well aligned to louver 5 and impinges on the front surface preventing a strong shear layer from forming at the leading edge. By the time the flow comes out of louver 5, it is nearly parallel to the louver direction, and facilitates the formation

[4] The peak magnitude of the power spectrum is an indication of the order of magnitude of fluctuations about the mean.

[5] Although we show the frequency spectra in the louver wakes, equivalent spectra near the louver surface exhibit the same general spectral characteristics. This is true for all Reynolds numbers.

[6] Front surface is used to denote the face which faces the flow vs back surface, which does not face the oncoming flow.

[7] However, in general the vortices on the back surfaces of the louvers are always stronger than those on the front surface.

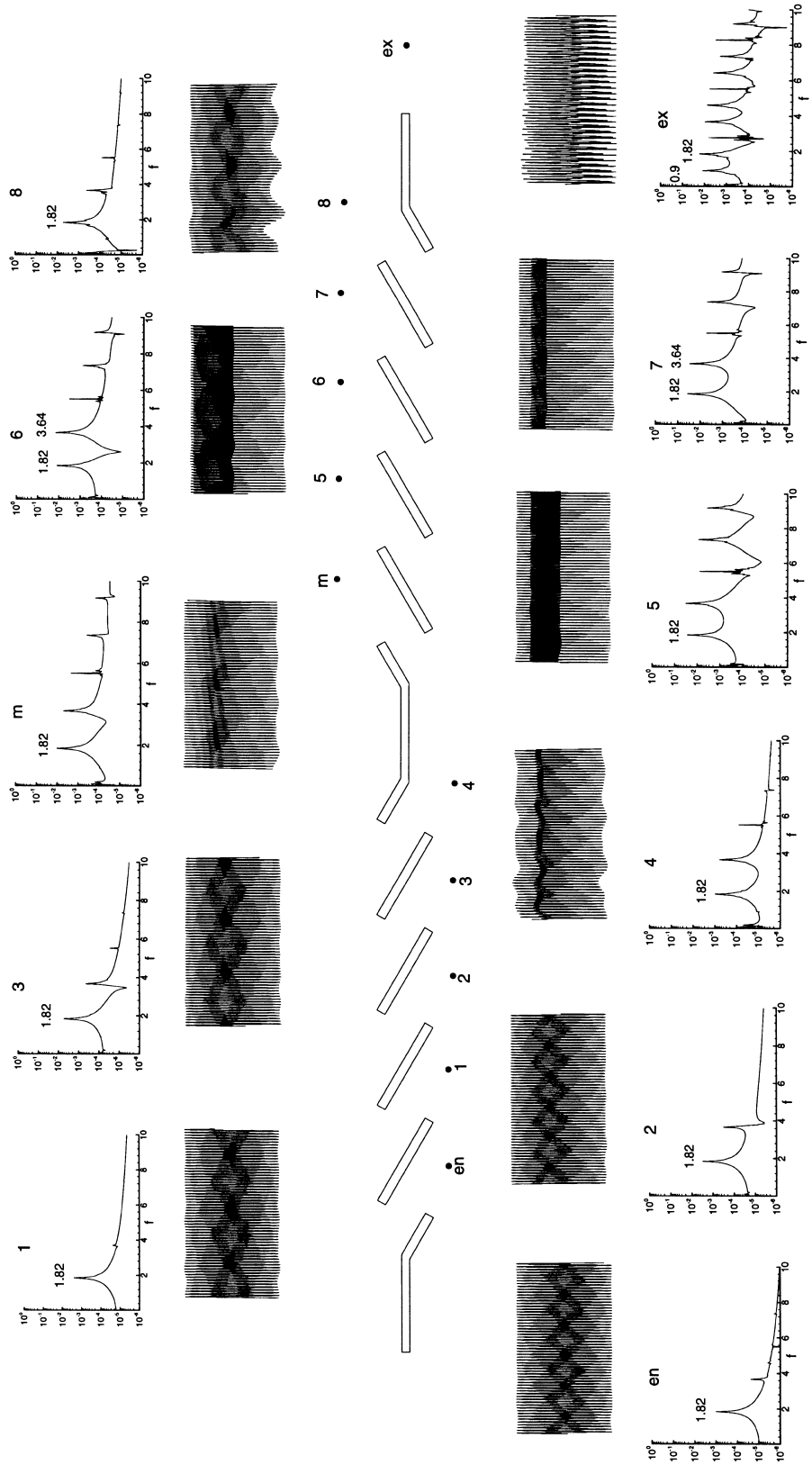

Fig. 9. Spatial distribution of frequency spectra of temperature at $Re_{in} = 1100$.

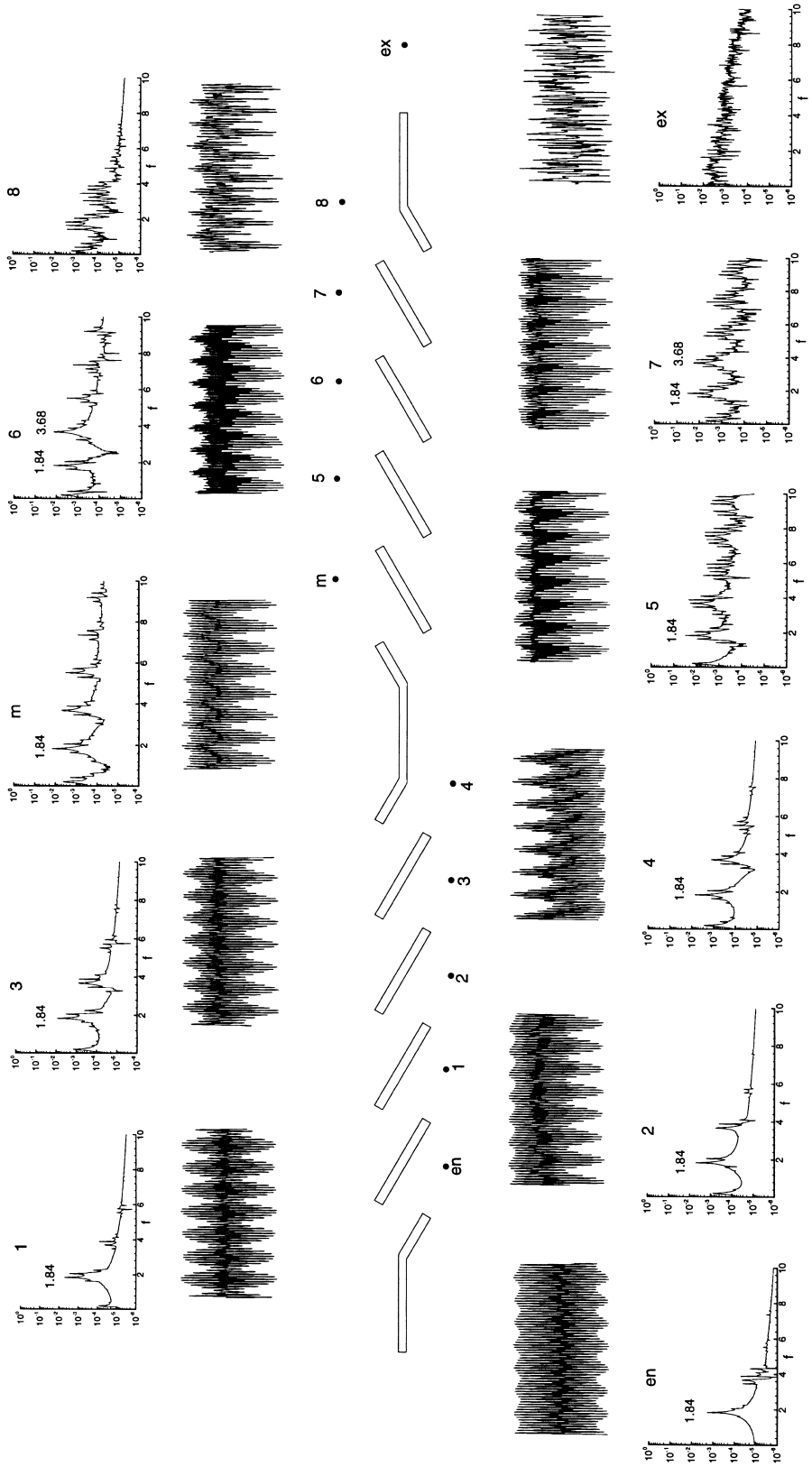

Fig. 10. Spatial distribution of frequency spectra of temperature at $Re_{in} = 1200$.

of leading edge shear layer instabilities on both sides of the louver.

In uniform flow over blunt plates [25], the Kelvin–Helmholtz instability is preceded by massive but steady separation and reattachment. However, an important facet to the observed transition in this study is the complete absence of any separation and reattachment on these louvers at prior Reynolds numbers. This, and the observed propagation of the exit wake instability into the array, leads us to conclude that the Kelvin–Helmholtz instability is influenced and accelerated by the original wake instability at the exit louver. The initiation of vortex shedding in louvered fin arrays at this Reynolds number has been observed in the flow visualization experiments of Howard [6]. In agreement with the present simulations, Howard [6] also found that the vortex shedding was initiated at the exit end of the array and the instability progressed upstream as the Reynolds number increased. Similar observations were reported by Mochzuki et al. [26] in their flow visualization studies of offset-strip fins, in which they found that the onset of vortex shedding moved upstream into the array from the trailing edge. Further, frequency measurements by Springer and Thole [7] in a multilouvered fin array, also showed that vortex shedding was present in the array at $Re_{in} = 1000$, but was not evident at $Re_{in} \leq 900$. Their measured fundamental frequency based on louver thickness and local mean flow velocity parallel to the louver of 0.17 agrees well with the current computed value. Normalizing the characteristic frequency with louver thickness and maximum mean flow velocity in the array (flow area corrected for obstruction caused by projected louver thickness), the characteristic frequency for the leading edge instability reduces to the value of 0.16. Zhang [27] has also obtained characteristic frequencies ranging from 0.14 to 0.17 in his numerical studies of infinite arrays of inline and staggered parallel fins. The corresponding characteristic frequency observed in the reattachment zone of blunt rectangular plates is 0.1 (based on approach velocity and plate thickness) by Tafti and Vanka [17] at $Re = 1000$, 0.12 by Kiya and Sasaki [28] at $Re = 26{,}000$, and 0.14 at $Re = 32{,}000$ by Cherry et al. [29].[8]

At $Re_{in} = 900$, leading edge vortex shedding is visibly established at the exit louver. The original wake instability still persists at the exit louver but now the fundamental and first harmonic in the wake assume values in synchronization with the Kelvin–Helmholtz instability in the interior. There is a distinct shift in the characteristic exit wake frequency from $f = 0.94$ to 0.86 and from $f_1 = 1.84$ to 1.70 between $Re_{in} = 800$ and 900. This is captured very clearly in flow visualization over one typical shedding cycle of the wake instability and in the frequency power spectrum on the top and bottom surface of the exit louver. Fig. 8 shows instantaneous vorticity contours and the power spectra for locations near the top and bottom surface of the exit louver and the wake. At the exit louver, in addition to the leading edge vortex shedding, a wake vortex at the trailing edge is also seen. The spectral characteristics at the locations on the exit louver (1 and 2 in Fig. 7(a)) are dominated by the Kelvin–Helmholtz instability occurring at the leading edge, as in the interior of the array, and it is only in the wake that we find the presence of $f = 0.86$.

As the Reynolds number increases to 1000, the *classification* of instabilities as they move upstream into the array becomes difficult. At this Reynolds number, the wake of louver 4 and the re-direction louver exhibit a wavy character. At the same time, leading edge free shear layer instabilities develop on both sides of louver 6 with the initiation of vortex shedding. Further, we also find a small recirculation zone form on the bottom leading edge of the redirection louver. The characteristic frequencies in the interior and the exit wake do not exhibit any change from their values at $Re_{in} = 900$. As the Reynolds number increases to 1100, the instability moves further upstream and initiates vortex shedding at the redirection louver on both, top and bottom faces. Further, a small recirculation zone forms at the front leading edge of louver 4. The spatial distribution of frequency spectra is shown in Fig. 9. Once again, we observe a change in the characteristic frequencies throughout the interior of the array and the exit wake. In the interior of the array, the characteristic frequency changes from 1.7 to 1.82, and correspondingly the wake frequency from $f = 0.86$ to 0.9 and from $f_1 = 1.7$ to 1.82. Curiously, at this Reynolds number the time signals and corresponding spectra are very well defined, with sharp spectral peaks, which is in contrast to the spectral distributions at $Re_{in} = 900$ and 1000. At $Re_{in} = 1200$, we observe additional recirculation regions, albeit quite small, at the entrance louver, on the front leading edge of louver 2, and the back leading edge of louver 3, as shown in Fig. 2. Fig. 10 shows the spectral distribution at $Re_{in} = 1200$. The flow in the exit wake has transitioned to a near chaotic state as evidenced by the absence of any strong spectral peaks. As the Reynolds number increases further to $Re_{in} = 1300$, leading edge instabilities with vortex shedding develop on both sides of louver 3 and on the front surface of louver 4. Fig. 11

[8] For louver directed flow, the comparison with blunt rectangular plate leading edge instability in a uniform flow is somewhat justified. However, we note that in uniform flow, the instability arises at a much higher Reynolds (350 based on plate thickness) than in the current calculation (90 based on plate thickness).

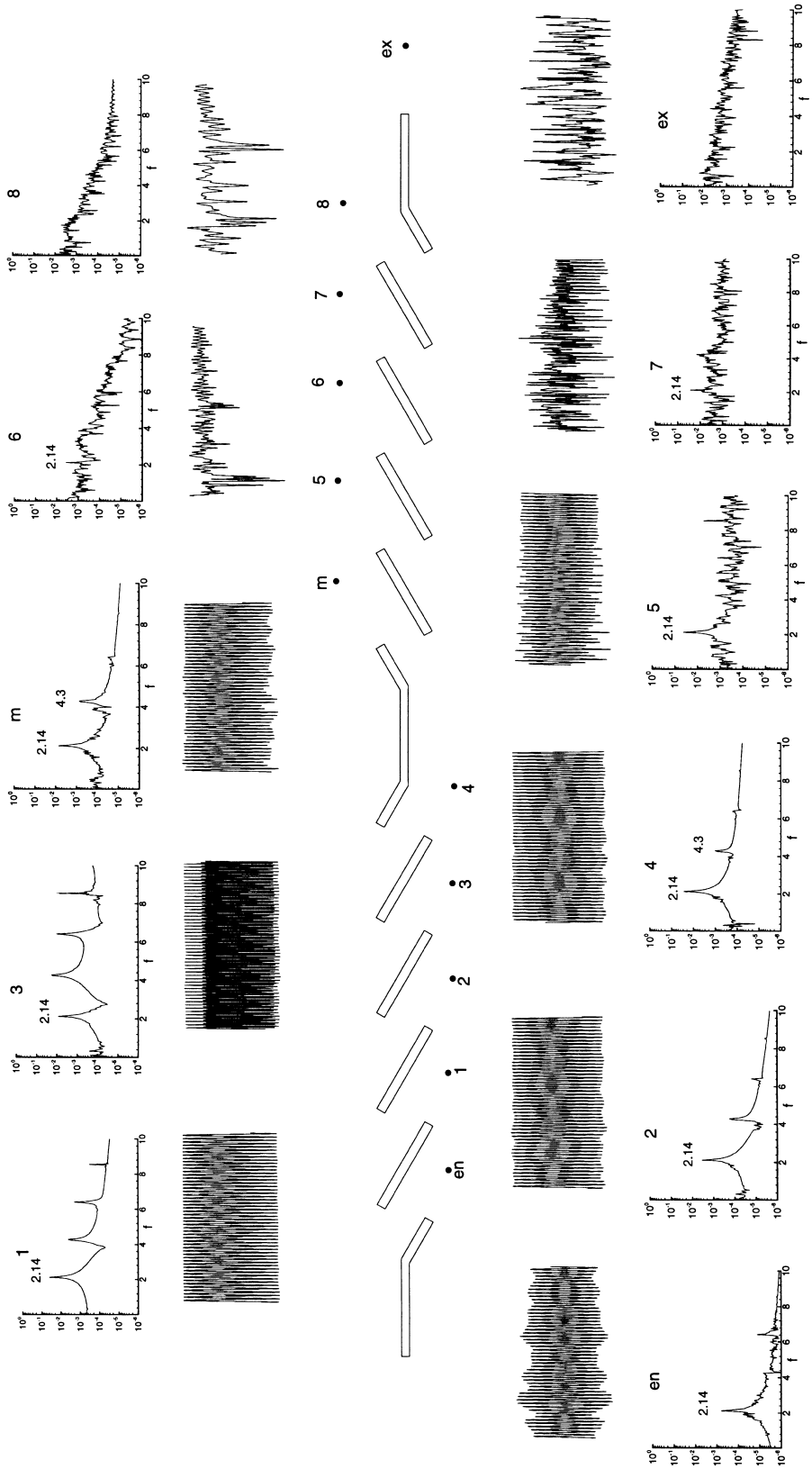

Fig. 11. Spatial distribution of frequency spectra of temperature at $Re_{in} = 1300$.

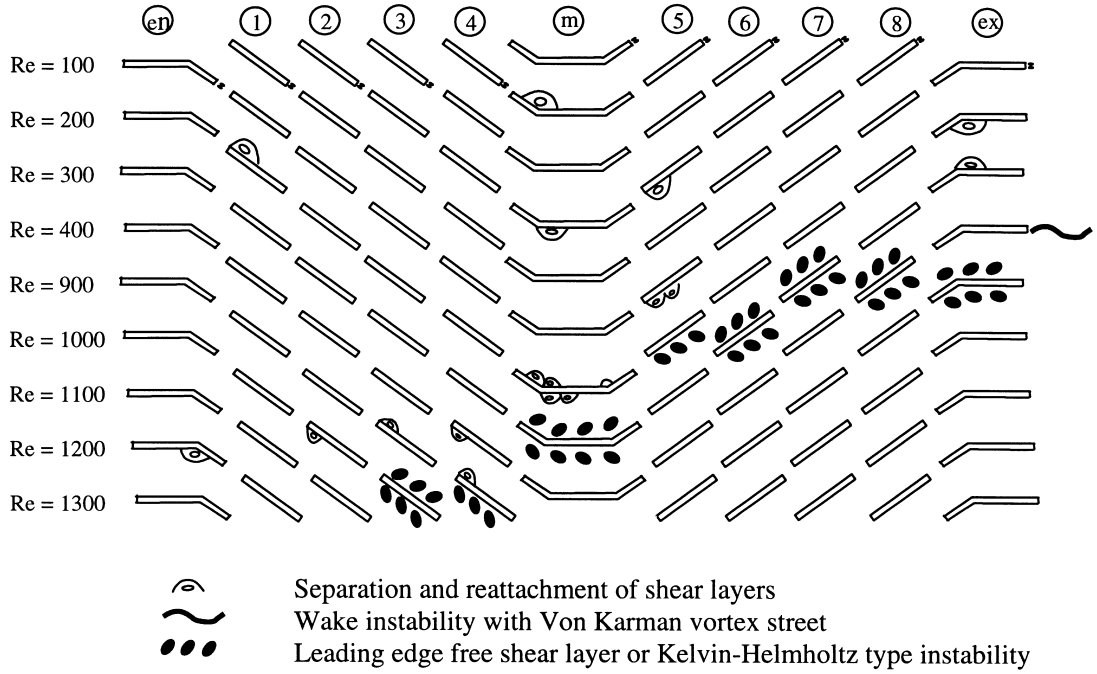

Fig. 12. Development and propagation of instabilities in the multilouvered geometry with a grid resolution of 64×64 per computational block. Only the initial appearance of instabilities is shown.

shows the spectral distribution in the array. We again observe a discrete change in the characteristic frequency from 1.84 at $Re_{in} = 1200$ to 2.14 at $Re_{in} = 1300$ and the flow tends towards a chaotic state in the downstream half of the array.

We note that in the range of Reynolds numbers studied, which is fairly typical of real applications, once the initial instability is established there is no clear demarcation between steady laminar, unsteady laminar and chaotic flow. In fact, there is a strong case to be made that all three regimes co-exist in the array. This observation has important implications on the use of the RANS approach with turbulence models. Although sophisticated models can account for these effects in an averaged sense, their universality and accuracy have limitations. Further, we also note that in our study we could not differentiate the impinging shear layer instability (ISLI), which was identified in the introduction as one the potential instabilities which could exist in the array. In the previous study of Nakamura et al. [22], the ISLI instability appeared at $Re = 250$ based on plate thickness, which is much higher than the equivalent maximum Reynolds number in this study. It is also not clear how this instability would manifest itself in the current study, in which the length-to-thickness ratio is fixed (at 10) and the Reynolds number varies. In the current setting, even if the instability were present it would not manifest itself with characteristic step changes in Strouhal number but an increase in Strouhal number vs Reynolds number. For instance, from Nakamura et al. [22], the Strouhal number varies between 1.5 and 2 for a length-to-thickness ratio of 10, between $Re_{in} = 2500$ and 10,000. Although, the current range of Reynolds numbers is much lower, the frequencies found in the interior are comparable. However, we suspect that the ISLI instability does not play a major role in the multi-louvered array.

5. Grid dependency study

The above calculations were repeated on a coarser grid of 64×64 per computational block. The intent was to study how closely the coarse mesh reproduced the results on the fine mesh. A close match between the two, would indicate the adequacy of the 96×96 mesh presented in this paper. Fig. 12 summarizes the transitional characteristics observed on the coarse mesh. On comparison with Fig. 2, we find that there are no major discrepancies between the two that would cast doubt on the veracity of the results on the fine mesh. The development and propagation of the main instabilities in the array are captured faithfully by the coarse mesh. The initial wake instability appears at $Re_{in} = 400$ with a characteristic frequency of 0.8125 (vs 0.84 on the fine mesh). The propagation of this instability into the interior of the array follows a trend

similar to the fine mesh. There are some differences between the two meshes during the initiation of the Kelvin–Helmholtz instability in the interior of the array. On the coarse mesh, the initiation of the instability is slightly delayed than on the fine mesh. However, the actual instability appears at the same Reynolds number of $Re_{in} = 900$ on louvers 7, 8 (vs louvers 5, 7, 8 on the fine mesh) and the exit louver. The initiation of leading edge vortex shedding from louver 5 is delayed till $Re_{in} = 1000$ on the coarse mesh. Similarly, the initiation of vortex shedding on the redirection louver is also delayed till $Re_{in} = 1200$ (vs $Re_{in} = 1100$ on the fine mesh). The characteristic frequency of vortex shedding at $Re_{in} = 900$ is observed to be 1.875 vs 1.7 on the fine mesh. Besides these minor differences, we did not observe any major discrepancies in the basic mechanism of the propagation of instabilities, which would warrant that a grid finer than 96×96 per block be used.

6. Conclusions

The paper describes the detailed transition mechanism in a multilouvered fin geometry. The initial instability appeared in the wake of the exit louver at a Reynolds number of 400 with a characteristic non-dimensional frequency of 0.84. It was found that the initial wake instability propagated inside the array as the Reynolds number increased. For Reynolds numbers between 600 and 700, power spectra in the interior (near the exit) of the array indicated an increase in energy near the first harmonic of the initial exit wake instability. By a Reynolds number of 900, free shear layer or Kelvin–Helmholtz type instabilities had developed on the leading edge of louvers near the exit. These instabilities had a characteristic non-dimensional frequency of 1.7. Once this happened, the exit wake switched frequencies in sympathy with the upstream Kelvin–Helmholtz instability. Similar, discrete changes in characteristic frequencies were observed on two other occasions as the instability moved upstream into the array. It was also observed that there existed a single characteristic frequency on all louvers at a given Reynolds number irrespective of whether vortex shedding was present on the louver.

We conclude by observing that this is the first study of its kind which has identified the transition in such detail. However, more studies are needed to study the effect of geometrical parameters, particularly the ratio of fin pitch to louver pitch and louver angle. For example, how would transition proceed if the louver geometry induced vortex shedding near the entrance to the louvered array? What scaling laws do the characteristic frequencies follow? These are questions which can only be answered by studying the transition process in other louver geometries.

References

[1] C.J. Davenport, Heat transfer and flow friction characteristics of louvered heat exchanger surfaces, in: J. Taborek, G.F. Hewitt, N. Afgan (Eds.), Heat Exchangers: Theory and Practice, Hemisphere, Washington DC, 1983, pp. 397–412.
[2] A. Achaichia, T.A. Cowell, Heat transfer and pressure drop characteristics of flat tube and louvered plate fin surfaces, Experimental Thermal and Fluid Science 1 (1988) 147–157.
[3] L.W. Zhang, D.K. Tafti, F.M. Najjar, S. Balachandar, Computations of flow and heat transfer in parallel-plate fin heat exchangers on the CM-5: effects of flow unsteadiness and three-dimensionality, Int. J. Heat Mass Transfer 40 (1997) 1325–1341.
[4] L.W. Zhang, S. Balachandar, D.K. Tafti, F.M. Najjar, Heat transfer enhancement mechanism in inline and staggered parallel-plate fin heat exchangers, Int. J. Heat Mass Transfer 40 (10) (1997) 2307–2325.
[5] R.L. Webb, P. Trauger, Flow structure in the louvered fin heat exchanger geometry, Experimental Thermal and Fluid Science 4 (1991) 205–217.
[6] P. Howard, Preliminary report on flow visualization studies on a two-dimensional model of a louvered fin heat exchanger, Penn State Project Report, 1987.
[7] M. Springer, K.A. Thole, Experimental design for flowfield studies of louvered fins, Experimental Thermal and Fluid Science 18 (1998) 258–269.
[8] A. Achaichia, T.A. Cowell, A finite difference analysis of fully developed periodic laminar flow in inclined louvered arrays. In: Proceedings of Second UK National Heat Transfer Conference, Glasgow, 1988. 2. p. 883–888.
[9] D.W. Halt, V.J. Allan, G.R. Fish, CFD applications of automotive heat exchangers. In: Proceedings of the ASME Fluid Engineering Division, ASME, 1996. FED-242. p. 175–180.
[10] M. Hiramatsu, T. Ishimaru, K. Matsuzaki, Research on fins for air conditioning heat exchangers (first report, numerical analysis of heat transfer on louvered fins), JSME International Journal, Series II 33 (4) (1990) Paper No. 88–1254 A.
[11] K. Suga, H. Aoki, Numerical study on heat transfer and pressure drop in multi-louvered fins, ASME/JSME Thermal Engineering Proceedings 4 (1991) 361–368.
[12] K. Suga, H. Aoki, T. Shingawa, Numerical analysis on two dimensional flow and heat transfer of louvered fins using overlaid grids, JSME International Journal 33 (1990) 122–127.
[13] A. Achaichia, M.R. Heikal, Y. Sulaimna, T.A. Cowell, Numerical investigation of flow and friction in louver fin arrays. In: Proceedings of the Tenth International Heat Transfer Conference on Heat Transfer, 1994, vol. 4. p. 333–338.
[14] F.H. Albernathy, R.E. Kronauer, The formation of vortex streets, J. Fluid Mech. 13 (1962) 1–20.

[15] P.W. Bearman, D.M. Trueman, An investigation of the flow around rectangular cylinders, Aero. Q. 23 (1972) 229–237.
[16] J.C. Lane, R.I. Loehrke, Leading edge separation from a blunt plate at low Reynolds number, Trans. ASME J. Fluids Eng. 102 (1980) 494–496.
[17] D.K. Tafti, S.P. Vanka, A numerical study of flow separation and reattachment on a blunt plate, Physics of Fluids A 3 (1991) 1749–1759.
[18] D.K. Tafti, S.P. Vanka, A three-dimensional numerical study of flow separation and reattachment on a blunt plate, Physics of Fluids A 3 (1991) 2887–2909.
[19] A.N. Stokes, M.C. Welsh, Flow-resonant sound interaction in a duct containing a plate, II: square leading edge, J. Sound Vib. 104 (1986) 55–73.
[20] Y. Nakamura, Y. Ohya, H. Tsuruta, Experiments on vortex shedding from flat plates with square leading and trailing edges, J. Fluid Mech. 222 (1991) 437–447.
[21] Y. Ohya, Y. Nakamura, S. Ozono, H. Tsuruta, R. Nakayama, A numerical study of vortex shedding from flat plates with square leading and trailing edges, J. Fluid Mech. 236 (1992) 445–460.
[22] Y. Nakamura, Y. Ohya, S. Ozono, R. Nakayama, Experimental and numerical analysis of vortex shedding from elongated rectangular cylinders at low Reynolds numbers $200–10^3$, Journal of Wind Engineering and Industrial Aerodynamics 65 (1996) 301–308.
[23] J.F. Thompson, Z.U.A. Warsi, C.W. Mastin, in: Numerical Grid Generation, Foundations and Applications, Elsevier Science Publishing Co Inc, New York, NY, 1985.
[24] D.K. Tafti, L.W. Zhang, G. Wang, A time-dependent calculation procedure for fully developed and developing flow and heat transfer in louvered fin geometries, Numerical Heat Transfer, Part A 35 (1999) 225–249.
[25] K. Sasaki, M. Kiya, Three-dimensional vortex structure in a leading-edge sepration bubble at moderate Reynolds numbers, J. Fluids Engg. 113 (1991) 405–410.
[26] S. Mochizuki, Y. Tagi, W. Yang, Transport phenomenon in stacks of interrupted parallel-plate surfaces, Exp. Heat Transfer 1 (1987) 127–140.
[27] L.W. Zhang, A numerical study of flow and heat transfer in compact heat exchangers, PhD thesis, University of Illinois, Urbana, Illinois, 1996.
[28] M. Kiya, K. Sasaki, Structure of a turbulent separation bubble, J. Fluid Mech. 137 (1983) 83–113.
[29] N.J. Cherry, R. Hillier, M.E.M.P. Latour, Unsteady measurements in a separated and reattaching flow, J. Fluid Mech. 144 (1984) 13–46.